JACS
JOURNAL OF THE AMERICAN CHEMICAL SOCIETY

Article

pubs.acs.org/JACS

Absorption of Low-Energy UV Radiation by Human Telomere G-Quadruplexes Generates Long-Lived Guanine Radical Cations

Akos Banyasz,[†] Lara Martínez-Fernández,[‡] Clémence Balty,[†] Marion Perron,[†] Thierry Douki,[§] Roberto Improta,*[,†,‡] and Dimitra Markovitsi*[,†]

[†]LIDYL, CEA, CNRS, Université Paris-Saclay, F-91191 Gif-sur-Yvette, France

[‡]Istituto Biostrutture e Bioimmagini, Consiglio Nazionale delle Ricerche, Via Mezzocannone 16, I-80134 Napoli, Italy

[§]CEA, INAC-SyMMES Laboratoire des Lésions des Acides Nucléiques, F-38000 Grenoble, France

Supporting Information

ABSTRACT: Telomeres, which are involved in cell division, carcinogenesis, and aging and constitute important therapeutic targets, are prone to oxidative damage. This propensity has been correlated with the presence of guanine-rich sequences, capable of forming four-stranded DNA structures (G-quadruplexes). Here, we present the first study on oxidative damage of human telomere G-quadruplexes without mediation of external molecules. Our investigation has been performed for G-quadruplexes formed by folding of $GGG(TTAGGG)_3$ single strands in buffered solutions containing Na^+ cations (TEL21/Na^+). Associating nanosecond time-resolved spectroscopy and quantum mechanical calculations (TD-DFT), it focuses on the primary species, ejected electrons and guanine radicals, generated upon absorption of UV radiation directly by TEL21/Na^+. We show that, at 266 nm, corresponding to an energy significantly lower than the guanine ionization potential, the one-photon ionization quantum yield is 4.5×10^{-3}. This value is comparable to that of cyclobutane thymine dimers (the major UV-induced lesions) in genomic DNA; the quantum yield of these dimers in TEL21/Na^+ is found to be $(1.1 \pm 0.1) \times 10^{-3}$. The fate of guanine radicals, generated in equivalent concentration with that of ejected electrons, is followed over 5 orders of magnitude of time. Such a quantitative approach reveals that an important part of radical cation population survives up to a few milliseconds, whereas radical cations produced by chemical oxidants in various DNA systems are known to deprotonate, at most, within a few microseconds. Under the same experimental conditions, neither one-photon ionization nor long-lived radical cations are detected for the telomere repeat TTAGGG in single-stranded configuration, showing that secondary structure plays a key role in these processes. Finally, two types of deprotonated radicals are identified: on the one hand, $(G\text{-}H_2)^\bullet$ radicals, stable at early times, and on the other hand, $(G\text{-}H_1)^\bullet$ radicals, appearing within a few milliseconds and decaying with a time constant of ∼50 ms.

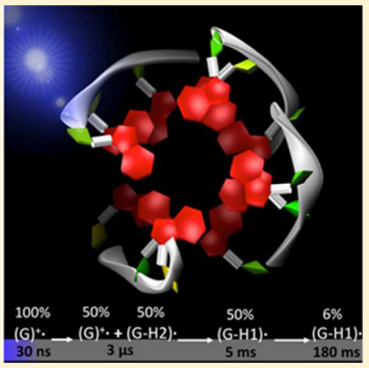

1. INTRODUCTION

Telomeres, DNA regions located at the chromosome ends of eukaryotic cells, play a key role in cell division.[1] Involved in aging and carcinogenesis, they constitute important therapeutic targets.[2] In humans, they are characterized by the presence of a repetitive base sequence, TTAGGG. Such guanine-rich repeats are capable of forming four-stranded structures (G-quadruplexes).[3] Both the existence of GGG runs and their folding in G-quadruplex structures have been correlated to the fact that telomeres are prone to oxidative damage.[4] The reason is that, among DNA bases, guanine has the lowest oxidation potential, which is further decreased upon stacking, rendering GGG triplets traps[5,6] for hole transfer[7−10] and preferential sites for redox reactions.[11]

So far, the studies that have addressed oxidative damage of G-quadruplexes deal exclusively with its occurrence via the action of other molecules.[12−18] However, guanine radicals, that are precursors to oxidative damage, may also be generated following absorption of UV radiation directly by DNA bases, provided that the energy of single photons is sufficiently high to eject an electron. Typically, this happens for wavelengths shorter than 200 nm.[19] Yet, it was recently shown that continuous UV irradiation of naked genomic DNA at 300 nm generates a well-known oxidation marker, 8-oxo-7,8-dihydro-2′-deoxyguanosine (8-oxoG), via a mechanism involving the guanine radical cation.[20] Although gas-phase experiments observed electron detachment from anionic DNA guanine runs by low-energy photons,[21,22] the direct UV-induced oxidation of G-quadruplexes in aqueous media, closer to biological environment, has never been examined.

The objective of the present work is to study the transient species, ejected electrons and resulting base radicals, triggered in G-quadruplexes by direct absorption of UV radiation. We focus on four-stranded structures formed by folding of the human telomeric sequence $GGG(TTAGGG)_3$ in phosphate buffer containing sodium cations (Figure 1a), abbreviated herein as TEL21/Na^+. Using nanosecond time-resolved

Received: June 8, 2017

DOI: 10.1021/jacs.7b05931
J. Am. Chem. Soc. XXXX, XXX, XXX−XXX

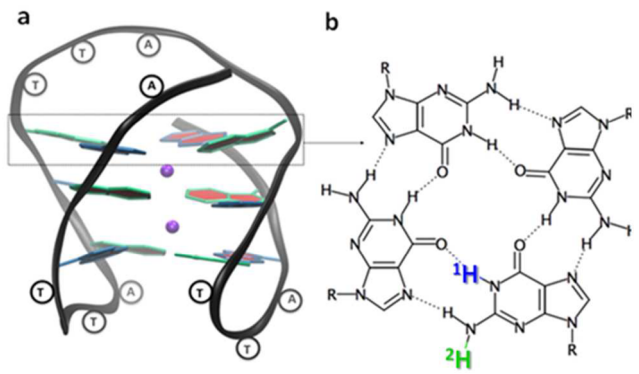

Figure 1. (a) TEL21/Na^+: G-quadruplex formed by the human telomeric sequence GGG(TTAGGG)$_3$ in the presence of Na^+ ions (violet). (b) Guanine tetrad: abstraction of protons ^{1}H or ^{2}H gives rise to deprotonated radicals (G-H1)$^\bullet$ or (G-H2)$^\bullet$, respectively.

absorption spectroscopy and quantum mechanical (TD-DFT)/molecular mechanics (QM/MM) calculations, we provide a global and quantitative picture of the ionization process. We show that the one-photon ionization quantum yield ϕ_{1i} at 266 nm, corresponding to an energy lower than the vertical guanine ionization potential by 2.7 eV,[23] is 4.5 × 10^{-3}. Such a quantum yield is comparable to that reported for cyclobutane pyrimidine dimers (CPDs) induced by direct UV absorption in naked genomic DNA,[24] indicating that this process could trigger important biological deregulation. Moreover, we show that about 35% of the guanine radical cations in TEL21/Na^+ disappears with a time constant of ca. 1 ms, which is over 3 orders of magnitude longer compared to what is reported in the literature for guanine radical cations produced by chemical oxidants in various DNA systems.[14,25,26] In the case of the telomere repeat TTAGGG in single stranded configuration, neither one-photon ionization nor long-lived radical cations generated by two-photon ionization are detected.

2. METHODOLOGICAL DETAILS

2.1. Materials. Oligonucleotides, HPLC purified, were purchased from Eurogentec Europe; their purity was tested by MALDI-TOF. They were dissolved in phosphate buffer (0.15 mol L^{-1} NaH_2PO_4, 0.15 mol L^{-1} Na_2HPO_4; pH 7). The purity of the buffer ingredients (Fluka) was higher than 99.999%. TEL21/Na^+ structures were prepared using a dry bath (Eppendorf-ThermoStatplus); 2 mL of concentrated GGG(TTAGGG)$_3$ in buffer solution was heated to 96 °C during 5 min, cooled down slowly to 4 °C, and maintained at this temperature overnight. Its absorption spectrum and melting curve are shown in Figure 2. For the preparation of TEL21/Na^+ solution at pH 3, the buffer concentration was diluted by a factor of 100; subsequently, the pH was adjusted by addition of a concentrated HCl solution. The absorption spectrum of TEL21/Na^+ at pH 3 is the same as for pH 7 (Figure 2a). TTAGGG solutions were heated to 96 °C for 5 min and rapidly cooled to 23 °C.

2.2. Time-Resolved Experiments. The excitation source was the fourth harmonic of a Nd:YAG laser (Spectra-Physics, Quanta Ray). The analyzing beam (150 W Xe-arc lamp, Applied Photophysics) passed through the sample at right angle with respect to the exciting beam, dispersed in a SPEX 270M monochromator, detected by a Hamamatsu R928 photomultiplier. An electrical discharge was applied to increase the Xe-arc intensity for detection of hydrated electrons. The excitation and detection optical path lengths were 0.1 and 1.0 cm, respectively. Fast shutters were placed in the path of exciting and probing beams in order to minimize sample exposure to both light sources. The excitation frequency was 0.2 Hz. The energy of the exciting pulse was measured by a pyroelectric sensor (OPHIR Nova2/PE25). For measurements on the sub-microsecond scale, solutions were contained in 10 × 10 mm spectroscopic cells and mildly stirred during the experiment. For longer times, ca. 40 mL of solution was circulated through a flow cell. Transient spectra were recorded using a wavelength-by-wavelength approach. The temperature of the solutions was maintained at 23 ± 0.5 °C. The absorbance of the samples at 266 nm, determined with a PerkinElmer Lamda 900 spectrophotometer, was 2.4 ± 0.2 in 10 mm, corresponding to a TEL21/Na^+ concentration of 1.3 × 10^{-5} mol L^{-1}. At the maximum excitation intensity (2 MW cm^{-2}), the concentration of electrons ejected per laser pulse in the excited volume (0.06 cm^3) was 1.2 × 10^{-6} mol L^{-1}.

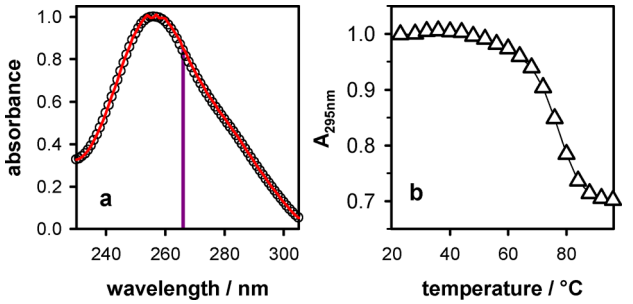

Figure 2. (a) Normalized absorption spectra of TEL21/Na^+ at pH 7 (black) and pH 3 (red). The vertical violet line indicates the wavelength of laser excitation. (b) Typical melting curve obtained for TEL21/Na^+ at pH 7.

2.3. Continuous Light Irradiations and Photoproduct Analysis. Continuous irradiations were performed using the Xe lamp of the SPEX spectrofluorimeter (bandwidth: 5 nm). During the irradiation the temperature of the solution, which was mildly stirred, was kept at 23 ± 0.1 °C. For the analysis of the markers, oligomers were enzymatically hydrolyzed to release unmodified bases as nucleosides and photoproducts as dinucleoside monophosphates. Two 2-h incubation periods were performed at 37 °C, first with phosphodiesterase II, DNase II, and Nuclease P1 (pH 6), and then with phosphodiesterase I and alkaline phosphatase (pH 8). The obtained solutions were analyzed by HPLC-MS/MS.[27] Specific quantification of the pyrimidine dimers and 8-oxoG was achieved by multiple reaction monitoring. In this detection mode, the first quadrupole of the mass spectrometer is set at the m/z value of the targeted pseudomolecular ion. Subsequently, these ions are directed into the second quadrupole, where they are fragmented by collision with molecular nitrogen. The resulting fragments are then directed into the third quadrupole that is set at m/z values specific for the targeted species.

2.4. Theoretical Calculations. All isolated species were studied at the Density Functional Theory (DFT) level, adopting M052X functional and 6-31G(d) basis set for geometry optimization; its time-dependent (TD) version was employed to characterize the excited electronic states and simulate the absorption spectra, increasing the basis set up to the 6-311+G(2d,2p) level. Bulk solvent effects were included by the Polarizable Continuum Model (PCM). The effect of solute/solvent hydrogen bonds was checked by explicitly including up to five water molecules of the first solvation shell. This computational approach has already been applied to the study of oligonucleotides,[28,29] including G-Quadruplexes,[30] providing a reliable description of their photophysical and photochemical behavior. Our analysis (see SI) shows that the conclusions provided by PCM/M052X/6-31G(d) are robust with respect to an increased basis set, inclusion of explicit water molecules, and the functional choice. Indeed, CAM-B3LYP computed spectra show the same features compared to those obtained at the M052X level. G-quadruplexes were treated at the Quantum Mechanical/Molecular Mechanics (QM/MM) level using the ONIOM interface[31] as implemented in Gaussian09.[32] We adopted the above-described QM approach for guanine bases and the inner Na^+ cations, while for the phospho-deoxyribose backbone and the outer Na^+ cations we used the Amber parm96.dat Force Field.[33] In this case, the excited states were computed at the PCM/TD-M052X/6-

DOI: 10.1021/jacs.7b05931
J. Am. Chem. Soc. XXXX, XXX, XXX−XXX

31G(d) level; for the blue part of the spectra, requiring calculations of up to 140 excited states, we considered only eight bases, those adjacent to the radical species, at the QM level. In order to enable easier comparison with the experimental spectra, each transition was convoluted with a Gaussian with half width half-maximum of 0.30 eV, after being red-shifted by −0.6 eV. Such a shift accounts for all sources of inaccuracy in our calculations (basis set size, lack of vibrational/thermal effects, and functional); it was selected so that the computed vertical transition of the lowest energy bright excited state of dG in water coincides with the maximum of the experimental absorption band.

3. RESULTS

3.1. Ejected Electrons. UV-induced ionization of DNA leads to electron ejection. At the time scale of our experiment (resolution 30 ns), ejected electrons are hydrated. To quantify the ionization process we use their well-characterized absorption spectrum.[34]

The hydrated electrons decay with a lifetime of 0.42 μs (Figure 3a). Such a fast decay is due to their scavenging by the phosphate groups[35] of the buffer, whose concentration is much higher than that of TEL21/Na^+. In this way, the damage of the studied nucleic acids by the ejected electrons[36−38] is avoided. Moreover, nucleobase anions resulting from reactions with hydrated electrons[19,39] do not contribute to the transient absorption signals. We also stress that the presence of halides (such as NaCl, commonly used in phosphate buffer, or LiCl in which the G-quadruplex folding is disfavored[40,41]) in the solution was purposely avoided in these experiments because they may undergo UV-induced electron detachment.[42]

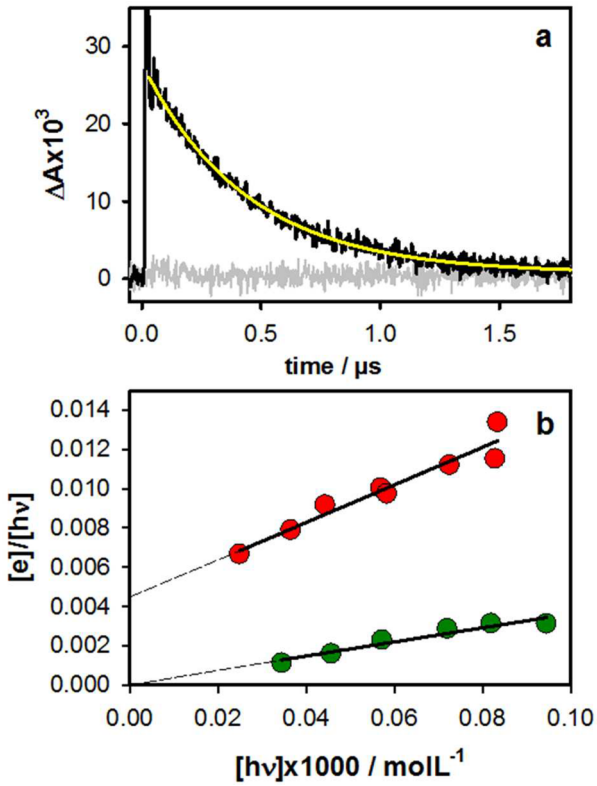

Figure 3. Quantification of ejected electrons. (a) Transient absorption signals determined at 700 nm upon laser excitation of TEL21/Na^+ in phosphate buffer (black) and the buffer alone (gray); the decay is fitted by a model function $c + \Delta A_0 \exp(-t/\tau)$, with τ = 0.42 μs (yellow). (b) Ionization curves obtained for TEL21/Na^+ (red) and TTAGGG (green); [e^-] and [$h\nu$] denote respectively the concentration of hydrated ejected electrons and absorbed photons per laser pulse; [e^-] is determined using the ΔA_0 values and a molar absorption coefficient of 19 700 mol^{-1} L cm^{-1}.[34] Experimental points (circles) are fitted with the linear function $[e^-]/[h\nu] = \phi_{1i} + \alpha[h\nu]$ (black).

The ionization plots of TEL21/Na^+ and TTAGGG, shown in Figure 3b, are obtained by varying the excitation intensity per laser pulse and, hence, the concentration of absorbed photons [$h\nu$]. The experimental electron concentrations divided by [$h\nu$] are plotted as a function of [$h\nu$] and fitted with a linear model function whose slope corresponds to two-photon ionization while the intercept on the vertical axis represents the quantum yield of one-photon ionization. Two-photon processes are observable for both systems. But only the G-quadruplex undergoes measurable one-photon ionization with a quantum yield of $(4.5 \pm 0.6) \times 10^{-3}$. Based on the sensitivity of our detection system, we judge that the ϕ_{1i} of TTAGGG is lower than 3×10^{-4}. No one-photon ionization is detected for thymine single strands,[43] while the ϕ_{1i} determined under the same experimental conditions for A-tracts in single- and double-stranded configurations is 4 times lower than that found here for TEL21/Na^+.[44]

3.2. Oxidation and Dimerization Markers. The full characterization of final UV-induced oxidation products is out of the scope of the present study. Yet, in order to compare the TEL21/Na^+ behavior with what was reported recently for naked genomic DNA,[20] we searched the fingerprint of 8-oxoG following irradiation with a continuous light source at 266 nm. We also quantified thymine dimerization markers, CPDs and pyrimidine(6-4) pyrimidone adducts (64PPs).

Analysis by HPLC coupled to mass spectrometry revealed indeed the presence of 8-oxoG (Figure 4a). The quantum yield

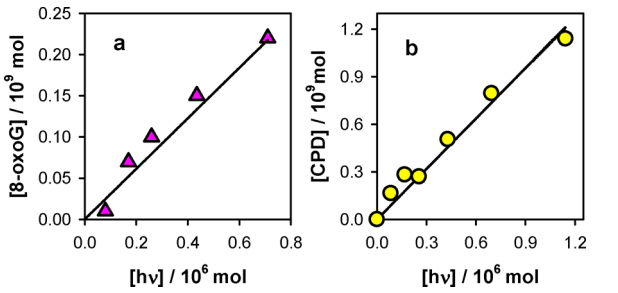

Figure 4. 8-oxoG (a) and CPDs (b) induced in TEL21/Na^+ as a function of absorbed photons upon irradiation at 266 nm with a continuous light source of oxygen saturated solutions. Black lines correspond to fits with linear functions $y = \phi[h\nu]$.

is $(3.2 \pm 0.3) \times 10^{-4}$, which amounts to about 7% of ϕ_{1i}. This shows that 8-oxoG is only a minor oxidation product in telomeric G-quadruplexes. However, it is significantly higher than that reported found for naked genomic DNA irradiated at 254 or 295 nm (5×10^{-5}).[20] No 8-oxoG was detected following continuous irradiation of argon saturated TEL21/Na^+ solutions.

The CPD quantum yield in TEL21/Na^+ is $(1.1 \pm 0.1) \times 10^{-3}$ (Figure 4b), while a much lower value, of the order of 10^{-5}, was found for 64PPs. Thus, it appears that one-photon ionization, occurring with a quantum yield of $(4.5 \pm 0.6) \times 10^{-3}$, is the dominant UV-induced reaction in the studied G-quadruplexes.

3.3. Radicals in TTAGGG. The spectra recorded for TTAGGG do no exhibit any noticeable modification between

DOI: 10.1021/jacs.7b05931
J. Am. Chem. Soc. XXXX, XXX, XXX−XXX

3 and 80 μs. They strongly resemble to the spectrum of the deprotonated guanosine radical $(G\text{-}H1)^{\bullet}$ reported by Candeias and Steenken[45,46] (Figure 5a), in which a proton has been

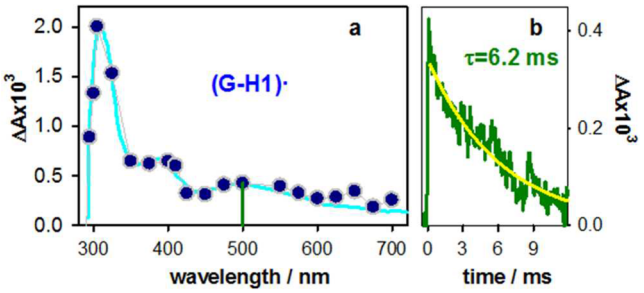

Figure 5. Transient absorption spectrum recorded for TTAGGG at 80 μs (a, circles) and signal decay at 500 nm (b, green). Excitation intensity: 2 MWcm^{-2}. The cyan line in (a) corresponds to the spectrum of monomeric guanosine radical $(G\text{-}H1)^{\bullet}$,[45] normalized at 500 nm with the spectrum of the single strand. The yellow line in (b) represents the fit with a mono-exponential function $c + \Delta A_0 \exp(-t/\tau)$.

abstracted from the nitrogen at position 1 of the guanine moiety (Figure 1b). The $(G\text{-}H1)^{\bullet}$ concentration, estimated from the differential absorbance (ΔA) at 500 nm and the molar absorption coefficient reported by Candeias and Steenken[45] (1500 mol^{-1} L cm^{-1}; Figure S1), is $(2.6 \pm 0.3) \times 10^{-3}$ molL^{-1}. This value is close to that of hydrated electrons determined for the same excitation intensity $(3.3 \pm 0.3) \times 10^{-3}$ mol L^{-1}, showing that we have almost quantitative conversion of the initially formed radical cations to $(G\text{-}H1)^{\bullet}$ radicals. The transient absorption signal at 500 nm disappears with a time constant of 6.2 $\pm$ 0.3 ms (Figure 5b).

3.4. Radicals in TEL21/Na$^+$: General Picture. The picture arising from the TEL21/Na$^+$ transient spectra, shown in Figure 6, is much more complex compared to that found for TTAGGG. Initially, we observe two bands peaking around 315 and 600 nm and a shoulder around 400 nm. Within 5 μs, the UV peak loses 15% of its intensity; such a small, albeit detectable, decrease concerns the whole spectral region up to ca. 550 nm, while the red part of the spectrum remains unchanged. The 600 nm band, discussed in detail in section 3.5, disappears on the millisecond time scale. The spectra recorded between 5 and 30 ms are similar to that of monomeric $(G\text{-}H1)^{\bullet}$;[45] the population of this radical at 5 ms, estimated in the same way as for TTAGGG, corresponds to 50% of the ejected electrons.

The similarity of the TEL21/Na$^+$ transient spectrum at 5 ms with the monomer radical spectrum is not as good as that observed for the single strand. In particular we observe a long tail around 600−700 nm. In order to understand the reasons of these differences, we computed the absorption spectra of $(G\text{-}H1)^{\bullet}$ both for the monomer in aqueous solution and when it is included in TEL21/Na$^+$. The theoretical spectra of monomeric $(G\text{-}H1)^{\bullet}$ (see SI) reproduce well the main features of their experimental counterpart (Figure S1). Our calculations indicate that, although inclusion of $(G\text{-}H1)^{\bullet}$ in TEL21/Na$^+$ modifies the energy and the oscillator strength of the electronic transitions, we still observe two bands between 400 and 500 nm (Figure 7a). Moreover, the intensity of the red tail becomes more pronounced compared to the monomer spectrum.

The decay of the TEL21/Na$^+$ transient signal at 500 nm is much slower than that of the single strand. It can be

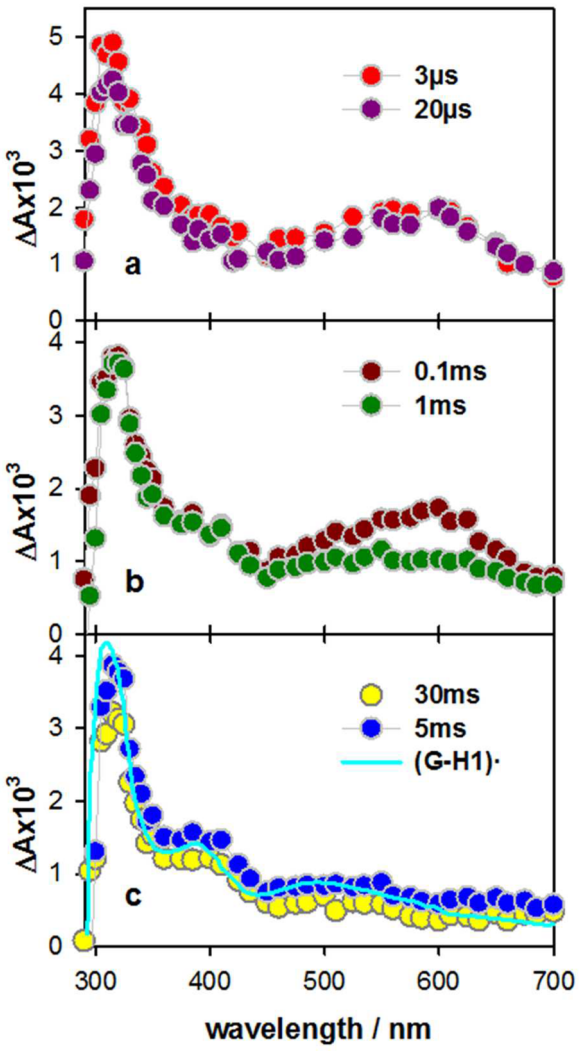

Figure 6. Transient absorption spectra (circles) recorded for TEL21/Na$^+$ at various times. Excitation intensity: 2 MWcm^{-2}. The cyan line corresponds to the spectrum of monomeric guanosine radicals $(G\text{-}H1)^{\bullet}$,[45] normalized at 500 nm with the spectrum at 5 ms.

approximated by the sum of two exponential functions with time constants of 1.2 $\pm$ 0.2 and 50 $\pm$ 10 ms. Similar time constants are found also for the signals recorded around 600 nm. The standard errors are derived from a large number of fits on data obtained for a series of independent measurements with different oligonucleotide batches. Typical decays and fits are shown in Figure 8. Details on the fitting procedure are given in the SI.

3.5. Radicals in TEL21/Na$^+$: Short Times. If the long time spectra of TEL21/Na$^+$ can be correlated to the $(G\text{-}H1)^{\bullet}$ radical, the assessment of early time spectra (Figure 6a) is not straightforward. The important width of the band at 600 nm (>0.8 eV fwhm) indicates the presence of at least two transient species. As they are not affected by the presence of oxygen, contribution from triplet excited states can be ruled out. $(G\text{-}H2)^{\bullet}$ radicals, from which a proton has been abstracted from the position 2 of guanine moiety (Figure 1b), absorb at 620 nm.[45,47,48] Indeed, the computed spectrum of $(G\text{-}H2)^{\bullet}$ shows a large absorption band in the 600−700 nm region (Figure 7b).

It is well documented that $(G\text{-}H2)^{\bullet}$ radicals are less stable than $(G\text{-}H1)^{\bullet}$ radicals in monomeric dG and dGMP,[45,47,48]

DOI: 10.1021/jacs.7b05931
J. Am. Chem. Soc. XXXX, XXX, XXX−XXX

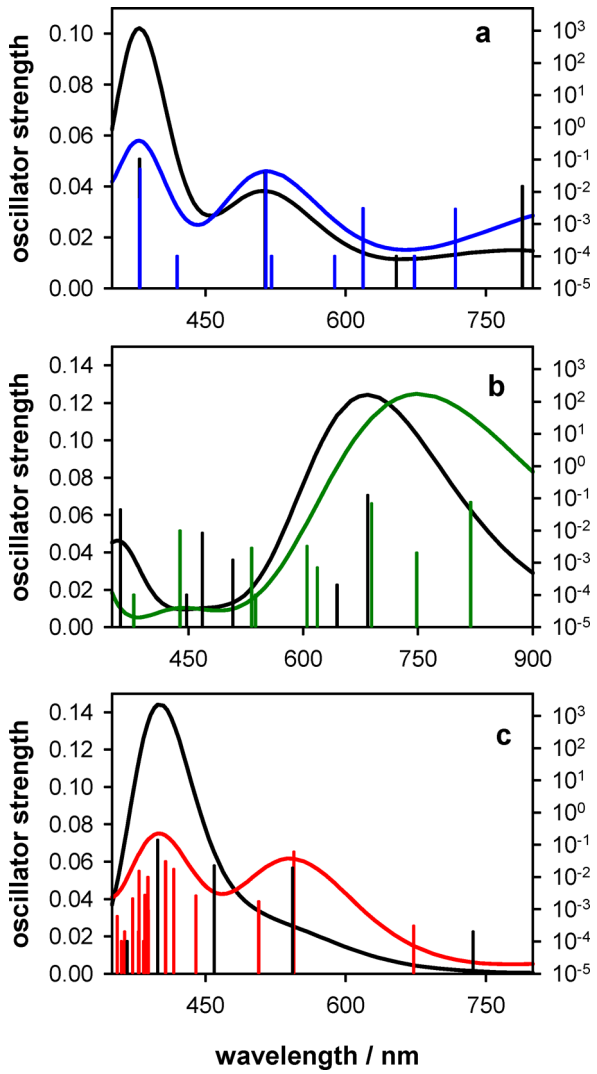

Figure 7. Spectra computed for guanine radicals in TEL21/Na^+ (colored lines) and isolated guanine in water (black lines). PCM/TD-M052x/6-31G(d)//M052x/6-31G(d) calculations: (a) $(G\text{-}H1)^{\bullet}$, (b) $(G\text{-}H2)^{\bullet}$, and (c) $(G)^{+\bullet}$. Sticks correspond to electronic transitions whose oscillator strength is shown on a logarithmic scale.

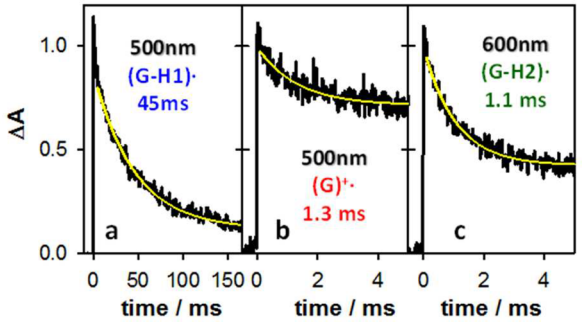

Figure 8. Decays of guanine radicals in TEL21/Na^+. Black lines: normalized experimental transient absorption signals. Yellow lines: fits with mono-exponential functions $c + \Delta A_0 \exp(-t/\tau)$. The time constants τ are indicated on each plot together with the dominant radical species.

(see also SI). Nevertheless, our calculations indicate that the relative stability is inverted in the case of TEL21/Na^+; the $(G\text{-}H2)^{\bullet}$ radical is 2.9 kcal/mol more stable than the $(G\text{-}H1)^{\bullet}$ radical. As a matter of fact, protons at position 1 of guanines are involved in Hoogsteen hydrogen bonding, whereas those at position 2 can be lost without affecting the hydrogen bond network of the tetrads (Figure 1b).

In the light of the above considerations, not only $(G\text{-}H2)^{\bullet}$ but also $(G)^{+\bullet}$ radicals should contribute to the transient spectrum at 3 μs. The latter can indeed be approximated (Figure 9) by a linear combination at a ratio 1:1 of the spectra

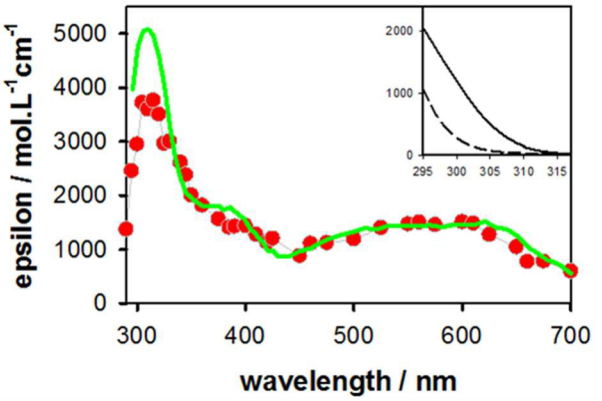

Figure 9. Spectrum recorded for TEL21/Na^+ at 3 μs (red circles); its absorbance has been divided by the concentration of ejected electrons. Green line: linear combination of the spectra reported for the monomeric $(G)^{+\bullet}$ and $(G\text{-}H2)^{\bullet}$(Figure S1[45]) at a ratio 1/1. Inset: steady-state absorption spectra of TEL21 (solid line) and dG (dashed line).

of these two radical species determined for monomeric guanosine, considering the respective molar absorption coefficients (Figure 9).[45] The molar absorption coefficient of the TEL21/Na^+ spectrum was obtained by dividing the differential absorbance at 3 μs by the initial concentration of photo-induced radicals, considered to be equal to that of ejected electrons under the same excitation conditions. The relatively lower intensity of the UV peak observed in the TEL21/Na^+ transient spectrum is due to the more intense ground-state absorption of G-quadruplexes below 315 nm (inset in Figure 9).

Further confirmation about our attribution of the radicals present in TEL21/Na^+ at 3 μs is obtained by decreasing the pH of the solution from 7 to 3, where deprotonation of the radical cation is hindered.[6,23] In acid environment, the 600 nm peak indeed disappears but the spectral shape below 500 nm remains the same as in neutral pH (Figure 10a). In Figure 10b we compare the spectrum TEL21/Na^+ at pH 3 with the spectrum of monomeric $(G)^{+\bullet}$. No dramatic differences are observed. However, in the case of G-quadruplex, the intensity of 400 nm band is similar to that at 500 nm, while, in the case of the monomer, it is clearly more intense. These trends are qualitatively reproduced in the spectra computed for the $(G)^{+\bullet}$ of the monomer and the G-quadruplex at the same level of calculations and arise from partial delocalization of the positive charge (Figures 7c).

4. DISCUSSION

The results presented in the previous section concern two different types of processes. On the one hand, one-photon ionization by low-energy UV radiation. On the other, the nature and the dynamics of the generated base radicals. For all

DOI: 10.1021/jacs.7b05931
J. Am. Chem. Soc. XXXX, XXX, XXX−XXX

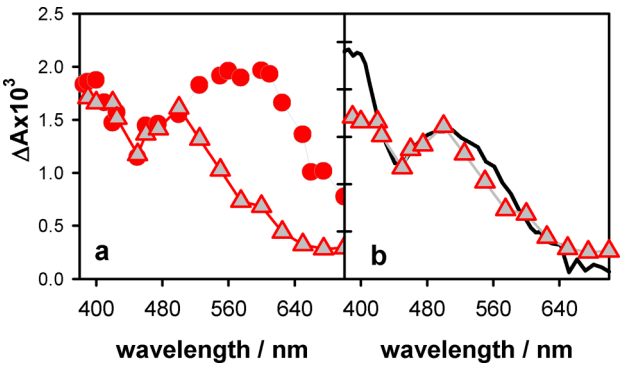

Figure 10. (a) Spectra recorded at 3 μs for TEL21/Na^+ at pH 7 (circles) and pH 3 (triangles; the intensity has been divided by 1.5). (b) Comparison of the TEL21/Na^+ spectrum at pH 3 with that of monomeric $(G)^{+\bullet}$ (from ref 45).

our measurements, the concentration of ejected electrons matches, within 10%, the radical concentration at 3 μs, the earliest time on which full transient absorption spectra were recorded. In this way, our study provides a global and quantitative picture of the primary species involved in the UV-induced oxidation of the studied systems. Below, we discuss the various aspects related to our study.

4.1. One-Photon Ionization. We showed in section 3.1 that the one-photon ionization quantum yield found for TEL21/Na^+ at 266 nm is $(4.5 \pm 0.6) \times 10^{-3}$, but it is lower than 3×10^{-4} for the telomere repeat TTAGGG. Yet, as we mentioned in the introduction, gas-phase experiments observed electron detachment by low-energy photons for short single stands.[22] From the study of various base sequences it appeared that the presence of guanine runs favors electron ejection. As gas-phase measurements were performed with partially deprotonated oligonucleotides and do not provide quantum yields, quantitative comparison with our results is not possible. In any case, we clearly showed that, in neutral aqueous solution, the propensity to undergo one-photon ionization is not due to the simple existence of GGG triplets in the base sequence and that the secondary structure plays a key role.

4.2. Nature of Generated Radicals. The species responsible for time-resolved spectra of both Tel21/Na^+ and TTAGGG (Figures 5 and 6) have been identified as guanine radicals. This means that, although AT dinucleotides may undergo photo-ionization at 266 nm,[49] radicals are eventually localized on guanines following charge transfer, as already reported for other modes of radical generation (direct excitation with high-energy photons or reactions involving electron acceptors) in various DNA systems.[12,14,46,50,51]

We detected three types of guanine radicals, resulting from deprotonation or tautomerization reactions:

reaction 1: deprotonation

$$(G)^{+\bullet} \rightarrow (G\text{-}H1)^{\bullet}$$

reaction 2: deprotonation

$$(G)^{+\bullet} \rightarrow (G\text{-}H2)^{\bullet}$$

reaction 3: tautomerization

$$(G\text{-}H2)^{\bullet} \rightarrow (G\text{-}H1)^{\bullet}$$

4.3. Fate of Radical Cations. The spectra obtained for TTAGGG show quantitative conversion of $(G)^{+\bullet}$ to $(G\text{-}H1)^{\bullet}$. We note that pulse radiolysis studies reported that reaction 1 in single and double strands takes place on the nanosecond time scale.[25,26]

In the case of TEL21/Na^+, we distinguish three different stages in the reaction of $(G)^{+\bullet}$:

Stage 1. At 3 μs, half of the $(G)^{+\bullet}$ population is still present while the other half has been converted to $(G\text{-}H2)^{\bullet}$ (reaction 2). This is derived from (i) the quantitative agreement between the G-quadruplex spectrum at 3 μs and that corresponding to an equimolar mixture of monomeric $(G)^{+\bullet}$ and $(G\text{-}H2)^{\bullet}$ radicals (Figure 9), (ii) the transient spectrum of TEL21/Na^+ at pH 3 (Figure 10), and (iii) the good agreement between the spectra computed for these species and the experimental ones (Figures 7b and 10b).

Stage 2. A few microseconds later additional 15% of the $(G)^{+\bullet}$ population disappear, as indicated by the intensity loss between 3 and 20 μs in the short-wavelength part of the spectrum (Figure 6a). But this disappearance is not due to deprotonation, because we do not see any concomitant intensity increase in the absorption spectra of $(G\text{-}H2)^{\bullet}$.

Stage 3. The remaining 35% of the $(G)^{+\bullet}$ population survives up to the millisecond time scale, decaying with a time constant of ~1 ms (Figure 8b). As a similar time constant has been found for the decay of $(G\text{-}H2)^{\bullet}$ (Figure 8c), it is not possible to identify the reaction path involved in this stage. It could be transformation to $(G\text{-}H1)^{\bullet}$ (reaction 1), which is the longest living radical (Figure 6c). Alternatively, $(G\text{-}H1)^{\bullet}$ could stem from $(G\text{-}H2)^{\bullet}$ (reaction 3), while $(G)^{+\bullet}$ gives rise to some reaction product absorbing further in the UV, being undetectable in our transient spectra.

The quasi-simultaneous disappearance, on the millisecond time scale, of $(G)^{+\bullet}$ and $(G\text{-}H2)^{\bullet}$ should be correlated with important conformational motions allowing breaking of hydrogen bonds and favoring configurations suitable for other reactions.

4.4. Comparison with Radicals Generated by Photosensitization. A recent article by Su and co-workers reported a study of guanine radicals in a series of G-quadruplexes using $SO_4^{-\bullet}$ radicals as photosensitizer.[14] They reported that deprotonation in G-quadruplexes is slower compared to duplexes, taking place within a few microseconds and leading to $(G\text{-}H2)^{\bullet}$ radicals (reaction 2). While our results are in qualitative agreement with these conclusions, there are noticeable differences. The photosensitization study[14] was focused on the formation of $(G\text{-}H2)^{\bullet}$ radicals, which was monitored on the microsecond time scale. Our study, in addition to detecting $(G\text{-}H2)^{\bullet}$ radicals, quantified the total radical population and explored their fate over much longer times (up to 180 ms), showing that the longest living species are $(G\text{-}H1)^{\bullet}$ radicals.

In more general way, the method used for radical generation is expected to affect their nature and their dynamics. Bimolecular electron transfer reactions in DNA depend on the accessibility of guanine sites;[52] the site of telomeric G-quadruplexes on which oxidation products are formed following bimolecular charge transfer where found to depend on the type of oxidant.[15] UV ionization of DNA bases in aqueous solvents is favored by well-stacked conformations.[43] Thus, we can speculate that bases of the inner tetrad in TEL21/Na^+ are more prone to photo-ionization giving rise to stabilized radical cations. Conformational factors, modulating, for example, the accessibility of water molecules, are also likely to play a role in the lifetime of deprotonated radical cations. Thus, the lifetime

DOI: 10.1021/jacs.7b05931
J. Am. Chem. Soc. XXXX, XXX, XXX−XXX

time of $(G\text{-}H1)^{\bullet}$ in TEL21/Na^+ is 45 ms (Figure 8a), versus only 6.2 ms in TTAGGG (Figure 5b).

4.5. 8-oxoG and Cyclobutane Thymine Dimers. As we explained in section 3.2, the objective of our work was not to characterize all the UV-induced lesions in TEL21/Na^+. We limited this part of our investigation to two markers. On the one hand, 8-oxoG; we found that the quantum yield of its formation, $(3.2 \pm 0.3) \times 10^{-4}$, is 1 order of magnitude higher than that determined for naked geneomic DNA.[20] On the other hand, we quantified CPDs and 64PPs showing that, electron ejection is 4 times more probable than thymine dimerization.

It is worth-noticing, although CPD formation in G-quadruplexes has been the subject of a few recent studies, both experimental[53−55] and theoretical,[56] no dimerization quantum yield has been reported so far. The CPD quantum found in our study, $(1.1 \pm 0.1) \times 10^{-3}$, is higher than that for reported for purifided calf thymus DNA ($\sim 0.6 \times 10^{-3}$),[24] in agreement with a hypersenitivity of human telomeres in respect to this lesion.[53]

5. CONCLUSIONS AND OUTLOOK

This first study on UV-induced ionization of G-quadruplexes led to two main conclusions. On the one hand, it revealed that direct absorption of low-energy UV irradiation is capable to provoke one-photon ionization in aqueous solution, giving rise to an equivalent population of guanine radicals. On the other hand, it showed that a significant population of radical cations may survive in these structures up to a few milliseconds.

Following the spectral evolution over several time scales and computing the spectra of the various guanine radicals included in four-stranded structures proved crucial in order to catch the complexity of radical transformations in such highly anisotropic systems undergoing dynamical conformational changes. This complexity is reflected in Figure 11, which summarizes the evolution of the population of the various types of guanine radicals in TEL21/Na^+, as discussed above.

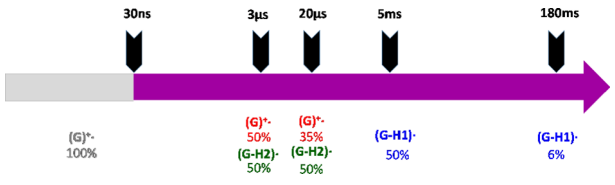

Figure 11. Population of guanine radicals in TEL21 as a function of time. Percentages correspond to the part of the initial radical population, equal to the population of ejected electrons.

Our results highlight the importance of the direct UV damage of telomeres, which is an intrinsic DNA property, versus the context dependent indirect damage mediated by other species. In addition to the biological relevance of our study, the spectral and dynamical features of guanine cations (electron holes) may be useful for the development of four-stranded guanine wires[57] whose functioning is based on charge transport.[12,58]

The present article, proposing an original approach for the study of charge generation in G-quadruplexes, raises a series of important questions. How do the structural factors (number of tetrads, topology, type of cations in the central cavity, etc.), already known to play a key role in the dynamics of excited-state relaxation,[59] affect one-photon ionization and the fate of the guanine radicals? Is the one-photon ionization quantum yield at longer wavelengths similar to that determined here for 266 nm? In this respect, it is worth-noticing that gas-phase experiments detected electron photodetachment from $[dG_6]^{-3}$ at 290 nm[22] and that the quantum yield found form the formation of 8-oxoG in naked genomic DNA is the same at 254 and 295 nm.[20] Moreover, it would be interesting to determine in a quantitative way the ensemble of oxidation products and correlate their formation with the various types of guanine radicals. Finally, we hope that our experimental findings will stimulate appropriate theoretical developments describing the mechanism of electron ejection at energies much lower than the ionization potential of the nucleobases.

■ ASSOCIATED CONTENT

Supporting Information

The Supporting Information is available free of charge on the ACS Publications website at DOI: 10.1021/jacs.7b05931.

Experimental absorption spectra of monomeric guanine radicals; fitting of transient absorption signals; computational details and additional results (PDF)

■ AUTHOR INFORMATION

Corresponding Authors

*robimp@unina.it

*dimitra.markovitsi@cea.fr

ORCID

Roberto Improta: 0000-0003-1004-195X

Dimitra Markovitsi: 0000-0002-2726-305X

Notes

The authors declare no competing financial interest.

■ ACKNOWLEDGMENTS

Financial support was received from the French National Research Agency (No. ANR-12-BS08-0001-01, OPHID project) and the CNRS-CNR PICS project (No. 6827-2015)/Bilateral CNR/CNRS. R.I. thanks the Université Paris-Saclay (Chaire d'Alembert No. 2016-10751).

■ REFERENCES

(1) Blackburn, E. H.; Epel, E. S.; Lin, J. *Science* **2015**, *350*, 1193−1198.

(2) Martinez, P.; Blasco, M. A. *J. Cell Biol.* **2017**, *216*, 875−887.

(3) Lipps, H. J.; Rhodes, D. *Trends Cell Biol.* **2009**, *19*, 414−422.

(4) Fouquerel, E.; Lormand, J.; Bose, A.; Lee, H. T.; Kim, G. S.; Li, J. F.; Sobol, R. W.; Freudenthal, B. D.; Myong, S.; Opresko, P. L. *Nat. Struct. Mol. Biol.* **2016**, *23*, 1092−1100.

(5) Meggers, E.; Michel-Beyerle, M. E.; Giese, B. *J. Am. Chem. Soc.* **1998**, *120*, 12950−12955.

(6) Saito, I.; Nakamura, T.; Nakatani, K.; Yoshioka, Y.; Yamaguchi, K.; Sugiyama, H. *J. Am. Chem. Soc.* **1998**, *120*, 12686−12687.

(7) Giese, B.; Amaudrut, J.; Köhler, A.-K.; Spormann, M.; Wessely, S. *Nature* **2001**, *412*, 318−320.

(8) Barnett, R. N.; Cleveland, C. L.; Joy, A.; Landman, U.; Schuster, G. B. *Science* **2001**, *294*, 567−571.

(9) Takada, T.; Kawai, K.; Fujitsuka, M.; Majima, T. *Proc. Natl. Acad. Sci. U. S. A.* **2004**, *101*, 14002−14006.

(10) Renaud, N.; Harris, M. A.; Singh, A. P. N.; Berlin, Y. A.; Ratner, M. A.; Wasielewski, M. R.; Lewis, F. D.; Grozema, F. C. *Nat. Chem.* **2016**, *8*, 1015−1021.

(11) Stemp, E. D. A.; Arkin, M. R.; Barton, J. K. *J. Am. Chem. Soc.* **1997**, *119*, 2921−2925.

(12) Choi, J.; Park, J.; Tanaka, A.; Park, M. J.; Jang, Y. J.; Fujitsuka, M.; Kim, S. K.; Majima, T. *Angew. Chem., Int. Ed.* **2013**, *52*, 1134−1138.

DOI: 10.1021/jacs.7b05931
J. Am. Chem. Soc. XXXX, XXX, XXX−XXX

(13) Delaney, S.; Barton, J. K. *Biochemistry* **2003**, *42*, 14159−14165.
(14) Wu, L. D.; Liu, K. H.; Jie, J. L.; Song, D.; Su, H. M. *J. Am. Chem. Soc.* **2015**, *137*, 259−266.
(15) Fleming, A. M.; Burrows, C. J. *Chem. Res. Toxicol.* **2013**, *26*, 593−607.
(16) Virgilio, A.; Esposito, V.; Mayol, L.; Giancola, C.; Petraccone, L.; Galeone, A. *Org. Biomol. Chem.* **2015**, *13*, 7421−7429.
(17) Szalai, V. A.; Singer, M. J.; Thorp, H. H. *J. Am. Chem. Soc.* **2002**, *124*, 1625−1631.
(18) Grygoryev, D.; Zimbrick, J. D. *Radiat. Res.* **2010**, *173*, 110−118.
(19) Candeias, L. P.; Steenken, S. *J. Am. Chem. Soc.* **1992**, *114*, 699−704.
(20) Gomez-Mendoza, M.; Banyasz, A.; Douki, T.; Markovitsi, D.; Ravanat, J. L. *J. Phys. Chem. Lett.* **2016**, *7*, 3945−3948.
(21) Yang, X.; Wang, X. B.; Vorpagel, E. R.; Wang, L. S. *Proc. Natl. Acad. Sci. U. S. A.* **2004**, *101*, 17588−17592.
(22) Gabelica, V.; Rosu, F.; Tabarin, T.; Kinet, C.; Antoine, R.; Broyer, M.; De Pauw, E.; Dugourd, P. *J. Am. Chem. Soc.* **2007**, *129*, 4706−4713.
(23) Schroeder, C. A.; Pluharova, E.; Seidel, R.; Schroeder, W. P.; Faubel, M.; Slavicek, P.; Winter, B.; Jungwirth, P.; Bradforth, S. E. *J. Am. Chem. Soc.* **2015**, *137*, 201−209.
(24) Douki, T. *J. Photochem. Photobiol., B* **2006**, *82*, 45−52.
(25) Kobayashi, K.; Tagawa, S. *J. Am. Chem. Soc.* **2003**, *125*, 10213−10218.
(26) Kobayashi, K.; Yamagami, R.; Tagawa, S. *J. Phys. Chem. B* **2008**, *112*, 10752−10757.
(27) Douki, T. *Photochem. Photobiol. Sci.* **2013**, *12*, 1286−1302.
(28) Improta, R.; Barone, V. *Top. Curr. Chem.* **2014**, *355*, 329−57.
(29) Improta, R.; Santoro, F.; Blancafort, L. *Chem. Rev.* **2016**, *116*, 3540−3593.
(30) Improta, R. *Chem. - Eur. J.* **2014**, *20*, 8106−8115.
(31) Dapprich, S.; Komaromi, I.; Byun, K. S.; Morokuma, K.; Frisch, M. J. *J. Mol. Struct.: THEOCHEM* **1999**, *461*, 1−21.
(32) Frisch, M. J.; Trucks, G. W.; Schlegel, H. B.; Scuseria, G. E.; Robb, M. A.; Cheeseman, J. R.; Scalmani, G.; Barone, V.; Mennucci, B.; Petersson, G. A.; Nakatsuji, H.; Caricato, M.; Li, X.; Hratchian, H. P.; Izmaylov, A. F.; Bloino, J.; Zheng, G.; Sonnenberg, J. L.; Hada, M.; Ehara, M.; Toyota, K.; Fukuda, R.; Hasegawa, J.; Ishida, M.; Nakajima, T.; Honda, Y.; Kitao, O.; Nakai, H.; Vreven, T.; Montgomery, J. A.; Peralta, J. J. E.; Ogliaro, F.; Bearpark, M.; Heyd, J. J.; Brothers, E.; Kudin, K. N.; Staroverov, V. N.; Kobayashi, R.; Normand, J.; Raghavachari, K.; Rendell, A.; Burant, J. C.; Iyengar, S. S.; Tomasi, J.; Cossi, M.; Rega, N.; Millam, J. M.; Klene, M.; Knox, J. E.; Cross, J. B.; Bakken, V.; Adamo, C.; Jaramillo, J.; Gomperts, R.; Stratmann, R. E.; Yazyev, O.; Austin, A. J.; Cammi, R. C.; Pomelli, C.; Ochterski, J. W.; Martin, R. L.; Morokuma, K.; Zakrzewski, V. G.; Voth, G. A.; Salvador, P.; Dannenberg, J. J.; Dapprich, S.; Daniels, A. D.; Farkas, O.; Foresman, J. B.; Ortiz, J. V.; Cioslowski, J.; Fox, D. J. *Gaussian 09*, revision A.02; Gaussian Inc.: Wallingford, CT, 2009.
(33) Cornell, W. D.; Cieplak, P.; Bayly, C. I.; Gould, I. R.; Merz, K. M.; Ferguson, D. M.; Spellmeyer, D. C.; Fox, T.; Caldwell, J. W.; Kollman, P. A. *J. Am. Chem. Soc.* **1995**, *117*, 5179−5197.
(34) Torche, F.; Marignier, J. L. *J. Phys. Chem. B* **2016**, *120*, 7201−7206.
(35) Buxton, G. V.; Greenstock, C. L.; Helman, W. P.; Ross, A. B. *J. Phys. Chem. Ref. Data* **1988**, *17*, 513−886.
(36) Behmand, B.; Wagner, J. R.; Sanche, L.; Hunting, D. J. *J. Phys. Chem. B* **2014**, *118*, 4803−4808.
(37) Sanche, L. *Radiat. Phys. Chem.* **2016**, *128*, 36−43.
(38) Nguyen, J.; Ma, Y.; Luo, T.; Bristow, R. G.; Jaffray, D. A.; Lu, Q.-B. *Proc. Natl. Acad. Sci. U. S. A.* **2011**, *108*, 11778−11783.
(39) Arce, R.; Rodriguez, G.; Singmaster, K. *Photochem. Photobiol.* **1983**, *38*, 631−637.
(40) Dao, N. T.; Haselsberger, R.; Michel-Beyerle, M. E.; Phan, A. T. *FEBS Lett.* **2011**, *585*, 3969−3977.
(41) Bhattacharyya, D.; Arachchilage, G. M.; Basu, S. *Front. Chem.* **2016**, *4*, 00038.
(42) Sauer, M. C.; Crowell, R. A.; Shkrob, I. A. *J. Phys. Chem. A* **2004**, *108*, 5490−5502.
(43) Marguet, S.; Markovitsi, D.; Talbot, F. *J. Phys. Chem. B* **2006**, *110*, 11037−11039.
(44) Banyasz, A.; Ketola, T.; Muñoz-Losa, A.; Rishi, S.; Adhikary, A.; Sevilla, M. D.; Martinez-Fernandez, L.; Improta, R.; Markovitsi, D. *J. Phys. Chem. Lett.* **2016**, *7*, 3949−3953.
(45) Candeias, L. P.; Steenken, S. *J. Am. Chem. Soc.* **1989**, *111*, 1094−1099.
(46) Candeias, L. P.; Steenken, S. *J. Am. Chem. Soc.* **1993**, *115*, 2437−2440.
(47) Chatgilialoglu, C.; Caminal, C.; Guerra, M.; Mulazzani, Q. G. *Angew. Chem., Int. Ed.* **2005**, *44*, 6030−6032.
(48) Chatgilialoglu, C.; Caminal, C.; Altieri, A.; Vougioukalakis, G. C.; Mulazzani, Q. G.; Gimisis, T.; Guerra, M. *J. Am. Chem. Soc.* **2006**, *128*, 13796−13805.
(49) Colon, L.; Crespo-Hernandez, C. E.; Oyola, R.; Garcia, C.; Arce, R. *J. Phys. Chem. B* **2006**, *110*, 15589−15596.
(50) Candeias, L. P.; O'Neill, P.; Jones, G. D. D.; Steenken, S. *Int. J. Radiat. Biol.* **1992**, *61*, 15−20.
(51) Rokhlenko, Y.; Cadet, J.; Geacintov, N. E.; Shafirovich, V. *J. Am. Chem. Soc.* **2014**, *136*, 5956−5962.
(52) Hall, J. P.; Poynton, F. E.; Keane, P. M.; Gurung, S. P.; Brazier, J. A.; Cardin, D. J.; Winter, G.; Gunnlaugsson, T.; Sazanovich, I. V.; Towrie, M.; Cardin, C. J.; Kelly, J. M.; Quinn, S. J. *Nat. Chem.* **2015**, *7*, 961−967.
(53) Rochette, P.; Brash, D. *PLoS Genet.* **2010**, *6*, e1000926.
(54) Su, D. G. T.; Fang, H. F.; Gross, M. L.; Taylor, J. S. A. *Proc. Natl. Acad. Sci. U. S. A.* **2009**, *106*, 12861−12866.
(55) Smith, J. E.; Lu, C.; Taylor, J. S. *Nucleic Acids Res.* **2014**, *42*, 5007−5019.
(56) Lee, W.; Matsika, S. *Phys. Chem. Chem. Phys.* **2017**, *19*, 3325−3336.
(57) Livshits, G. I.; Stern, A.; Rotem, D.; Borovok, N.; Eidelshtein, G.; Migliore, A.; Penzo, E.; Wind, S. J.; Di Felice, R.; Skourtis, S. S.; Cuevas, J. C.; Gurevich, L.; Kotlyar, A. B.; Porath, D. *Nat. Nanotechnol.* **2014**, *9*, 1040−1046.
(58) Thazhathveetil, A. K.; Harris, M. A.; Young, R. M.; Wasielewski, M. R.; Lewis, F. D. *J. Am. Chem. Soc.* **2017**, *139*, 1730−1733.
(59) Changenet-Barret, P.; Hua, Y.; Markovitsi, D. *Top. Curr. Chem.* **2014**, *356*, 183−202.

DOI: 10.1021/jacs.7b05931
J. Am. Chem. Soc. XXXX, XXX, XXX−XXX